

Contents lists available at ScienceDirect

Petroleum Science

journal homepage: www.keaipublishing.com/en/journals/petroleum-science



Original Paper

3D rock physics template-based probabilistic estimation of tight sandstone reservoir properties



Hao-Jie Pan ^a, Chao Wei ^{b, *}, Xin-Fei Yan ^b, Xiao-Ming Li ^b, Zhi-Fang Yang ^b, Zhi-Xian Gui ^{a, **}, Shu-Xian Liu ^a

- ^a College of Geophysics and Petroleum Resources, Yangtze University, Wuhan, 430100, Hubei, China
- ^b Research Institute of Petroleum Exploration and Department, Petrochina, Beijing, 100083, China

ARTICLE INFO

Article history: Received 6 April 2023 Received in revised form 24 September 2023 Accepted 18 April 2024 Available online 21 April 2024

Edited by Jie Hao and Meng-Jiao Zhou

Keywords:
Tight sandstones
Pore structure
3D rock physics template
Seismic inversion
Reservoir property estimation

ABSTRACT

Quantitative prediction of reservoir properties (e.g., gas saturation, porosity, and shale content) of tight reservoirs is of great significance for resource evaluation and well placements. However, the complex pore structures, poor pore connectivity, and uneven fluid distribution of tight sandstone reservoirs make the correlation between reservoir parameters and elastic properties more complicated and thus pose a major challenge in seismic reservoir characterization. We have developed a partially connected double porosity model to calculate elastic properties by considering the pore structure and connectivity, and to analyze these factors' influences on the elastic behaviors of tight sandstone reservoirs. The modeling results suggest that the bulk modulus is likely to be affected by the pore connectivity coefficient, while the shear modulus is sensitive to the volumetric fraction of stiff pores. By comparing the model predictions with the acoustic measurements of the dry and saturated quartz sandstone samples, the volumetric fraction of stiff pores and the pore connectivity coefficient can be determined. Based on the calibrated model, we have constructed a 3D rock physics template that accounts for the reservoir properties' impacts on the P-wave impedance, S-wave impedance, and density. The template combined with Bayesian inverse theory is used to quantify gas saturation, porosity, clay content, and their corresponding uncertainties from elastic parameters. The application of well-log and seismic data demonstrates that our 3D rock physics template-based probabilistic inversion approach performs well in predicting the spatial distribution of high-quality tight sandstone reservoirs in southwestern China. © 2024 The Authors. Publishing services by Elsevier B.V. on behalf of KeAi Communications Co. Ltd. This is an open access article under the CC BY-NC-ND license (http://creativecommons.org/licenses/by-nc-nd/ 4.0/).

1. Introduction

As an important unconventional hydrocarbon resource, tight sandstone reservoirs have low porosity, low permeability, high heterogeneity, non-uniform gas—water distribution, and complex pore structures. These features reduce the contrast between the elastic behaviors of hydrocarbon reservoirs and surrounding formations, which results in the multiplicity and uncertainty of seismic interpretation. Therefore, the key to accurately predicting reservoir properties relies on a reasonable relationship between reservoir characteristics and elastic responses of tight sandstone reservoirs.

E-mail addresses: cwei@petrochina.com.cn (C. Wei), gyy68@126.com (Z.-X. Gui).

Rock physics models that relate rock properties and microstructures to elastic properties provide physical bases for reservoir property estimation. Some authors have presented different theoretical models to characterize the elastic properties of tight sandstone reservoirs. According to the classification of Smith et al. (2009), Ruiz and Cheng (2010) divided the pore spaces into stiff pores with a relatively large aspect ratio and soft pores with a small aspect ratio. The authors proposed a soft-porosity model based on the self-consistent approximation (SCA) model to describe the elastic properties of tight reservoirs. Liu et al. (2015) developed a rock-physics modeling scheme based on the extended Raymer equation, SCA, and Gassmann equation to calculate the elastic moduli of tight sandstone reservoirs containing the disconnected pores. Yan et al. (2016) combined the Mori-Tanaka model (MT) with the Gassmann equation to establish a theoretical model for a partially connected porous medium.

^{*} Corresponding author.

^{**} Corresponding author.

More recently, Luo et al. (2019) introduced feldspar-related pores into the Xu—White model and proposed a multi-pore Xu—White model of tight sandstone reservoirs. Pan et al. (2020) developed a multi-pore Pride model by considering the complex pore structure and the consolidation of tight sandstone reservoirs. However, these models often allow for no more than two factors of the pore structure, pore connectivity, and partial fluid saturation. Consequently, the relationship between reservoir properties and elastic behaviors of tight sandstone reservoirs via theoretical modeling remains poorly characterized, which presents a challenge in reservoir prediction. It is therefore necessary to develop a theoretical model that sufficiently incorporates the mineral composition, pore fluids, and microstructures.

Rock physics template (RPT), directly relating the elastic parameters to reservoir parameters, has proven to be an effective tool for fluid identification and reservoir characterization. The classic 2D RPT based on the acoustic impedance and velocity ratio is unable to predict more than two of the reservoir parameters and thus fails to provide satisfactory estimations. By contrast, the 3D RPT considers the influences of porosity, water saturation, and shale content (or pore structure) on elastic responses, significantly improving reservoir property estimates' accuracy. Li and Zhang (2018) constructed a 3D RPT by combining the Gassmann equation and differential effective medium analytical model to predict gas saturation, pore aspect ratio and porosity from the seismic-inverted P-wave and S-wave impedances, and density for the carbonate reservoirs. Pan et al. (2019) proposed a 3D elastic-electrical RPT to estimate hydrate saturation, porosity, and shale content simultaneously. Pang et al. (2021) developed a multi-scale 3D RPT based on attenuation, impedance, and velocity ratio for tight sandstone reservoirs and predicted water saturation, porosity, and shale content from the laboratory, well-log, and seismic data. Tan et al. (2021) constructed a 3D RPT based on the equivalent inclusionaverage stress model for shale reservoirs and applied it to predict crack aspect ratio and quartz content from seismic-inverted elastic parameters. Unfortunately, such 3D RPTs combined with the deterministic optimization algorithm are often used to predict different types of reservoir properties and fail to quantify their corresponding uncertainties.

A 3D RPT-based probabilistic inversion method is proposed to overcome the problems mentioned earlier to predict reservoir properties from seismic-inverted elastic parameters. We first establish a partially connected double porosity model based on several effective medium theories and analyze the effects of pore structure and connectivity on elastic responses. Then, we construct a 3D RPT based on P-wave and S-wave impedances and density to quantitatively characterize tight sandstone reservoirs. Combined with Bayesian inverse theory, a 3D RPT calibrated with ultrasonic laboratory data is applied to predict the reservoir parameters and their uncertainties for tight sandstone reservoirs in central Sichuan.

2. Geological background

Sichuan Basin in the southwest of China is an important gasproducing region. Based on the basement properties, genetic types, and structural characteristics, it can be divided into five tectonic units (Li et al., 2017; Shen et al., 2021) (Fig. 1): 1) eastern Sichuan steep structural zone; 2) southern Sichuan gentle structural zone; 3) western Sichuan depression zone; 4) central Sichuan uplift zone; and 5) northern Sichuan flat folded zone. The Anyue gas field study area is located in the central Sichuan Basin. The Upper Triassic Xujiahe Formation is an important interval for developing tight sandstone gas reservoirs. It is commonly divided into six members from bottom to top according to their lithology, reservoir development, and sedimentary cycle (Zou et al., 2013; Lai

et al., 2016). The first, third, and fifth members are the source rocks composed of mudstones and shales. The second, fourth, and sixth members represent the reservoir rocks dominated by sandstones and conglomerates. Among them, the tight sandstone reservoirs in the second member are the intervals of interest, characterized by low permeability (0.01–1 mD), low porosity (5–10%), and high heterogeneity due to a series of mechanical compaction, cementation. and dissolution processes.

Apart from controlling the reservoir quality, diagenesis also has an appreciable impact on the microscopic characteristics, such as pore structures, connectivity, and fluid distribution. Thin-section analysis shows that the pore types in tight sandstone reservoirs of the second member mainly consist of the intergranular/intragranular dissolved pores and micro-cracks (Fig. 2). The former is generated by dissociating some unstable minerals, while the latter is generated by the hydrocarbon expulsion and geopressure evolution (Vernik and Landis, 1996). Such complex pore structures together with the clay/calcite cement might be the crucial factors affecting the pore connectivity, which further makes gas-water distribution more complicated. Therefore, the microscopic features, such as the pore structure and pore connectivity, as well as the gas-water distribution, should be taken into account when carrying out the rock physics modeling of tight sandstone reservoirs.

3. Rock physics modeling of tight sandstone reservoirs

3.1. Partially connected double porosity model

Considering that the tight sandstone reservoirs have poor pore connectivity, uneven gas—water distribution, and complex pore structure, we developed a partially connected double porosity model based on different effective medium theories to characterize elastic wave velocities. The main rock physics modeling procedure, as portrayed in Fig. 3, includes three parts: (1) calculating the elastic moduli of the rock matrix; (2) computing the elastic moduli of dry rock framework; (3) obtaining the elastic moduli of saturated rock.

3.1.1. Elastic moduli of the rock matrix

The tight sandstones are mainly composed of quartz and clay with a small amount of other minerals, such as feldspar and calcite. Then, the Voigt—Reuss—Hill (VRH) average (Hill, 1952) is used to calculate the bulk ($K_{\rm ma}$) and shear ($\mu_{\rm ma}$) moduli of the solid mineral mixture:

$$K_{\text{ma}} = \frac{1}{2} \left[\sum_{i=1}^{N} f_i K_i + \left(\sum_{i=1}^{N} f_i / K_i \right)^{-1} \right],$$
 (1)

$$\mu_{\text{ma}} = \frac{1}{2} \left[\sum_{i=1}^{N} f_i \mu_i + \left(\sum_{i=1}^{N} f_i / \mu_i \right)^{-1} \right], \tag{2}$$

where K_i and μ_i are the bulk and shear moduli of the *i*th mineral component, respectively; f_i is the volume fraction of the *i*th mineral component, and N is the total types of solid mineral components.

The unconnected pores, hindering the flow and exchange of pore fluids with the outside, are impermeable and treated as isolated pores embedded in a rock matrix (Liu et al., 2015). Assuming that the fractions of stiff and soft pores are the same for both isolated and connected parts, the SCA model can be used to obtain the bulk (K_0) and shear (μ_0) moduli of the rock matrix with the disconnected pores (Berryman, 1980):

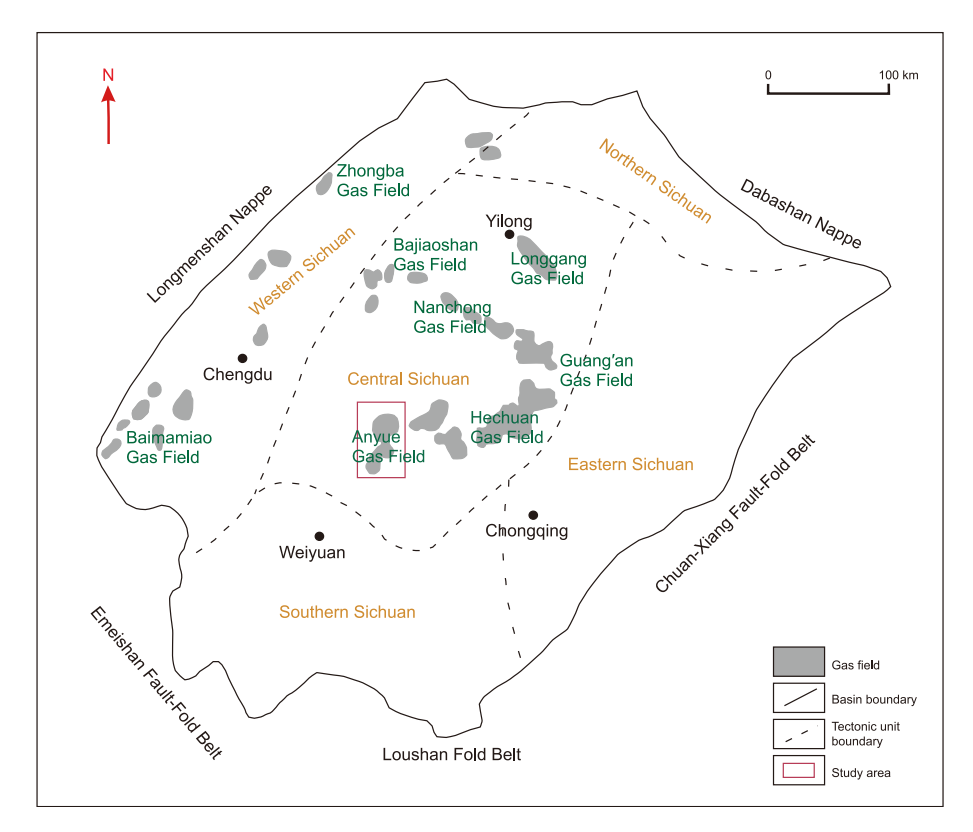


Fig. 1. The Sichuan Basin's tectonic divisions and the study area's location (after Shen et al., 2021).

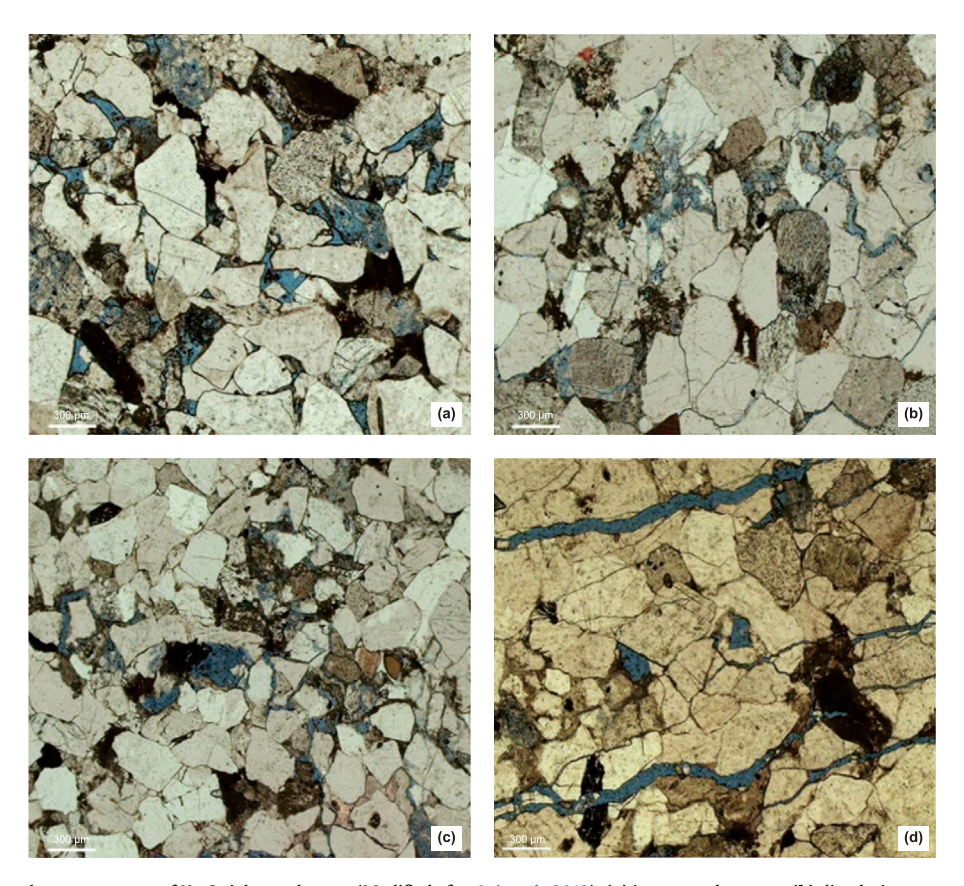


Fig. 2. Thin sections showing the pore systems of Xu-2 tight sandstones (Modified after Lai et al., 2018): (a) intergranular pores, (b) dissolution pores, (c) intragranular pores, and (d) micro-cracks.

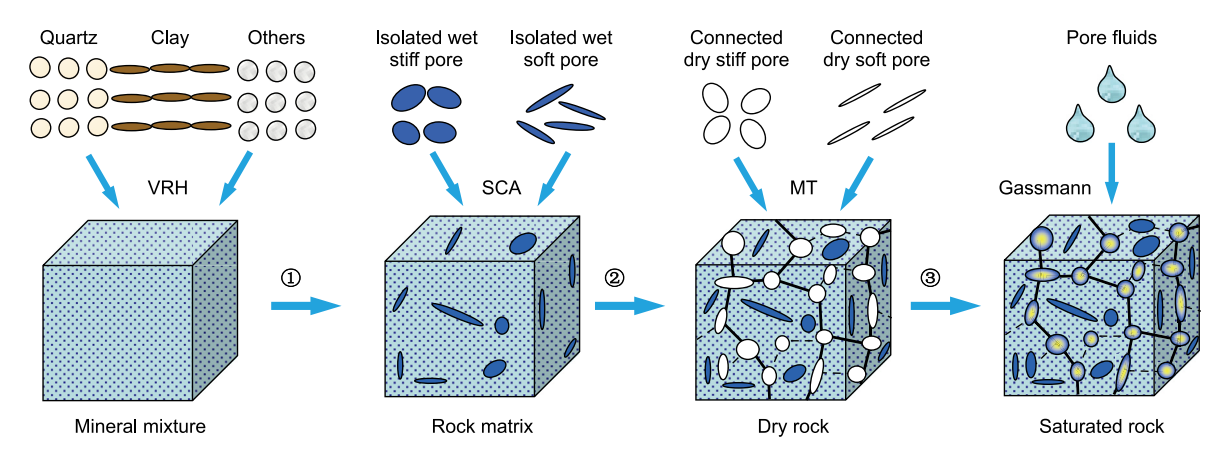


Fig. 3. Rock physics modeling scheme of tight sandstone reservoirs.

$$\frac{1-\varphi}{1-\eta\varphi}(K_{\text{ma}}-K_0)P_{\text{ma}} + \frac{(1-\eta)\varphi}{1-\eta\varphi} \sum_{i=1}^{M} x_i(K_{\text{w}}-K_0)P_{\text{w}}^i = 0,$$
 (3)

$$\frac{1-\varphi}{1-\eta\varphi}(\mu_{ma}-\mu_{0})Q_{ma} - \frac{(1-\eta)\varphi}{1-\eta\varphi}\sum_{i=1}^{M}x_{i}\mu_{0}Q_{w}^{i} = 0,$$
(4)

where φ is the total porosity; η is the connectivity coefficient; P_{ma} and Q_{ma} are the polarization factors of the rock matrix embedded by the solid mineral mixture; x_i represents the fraction of the isolated pore i; K_{w} is the bulk modulus of water; P_{w}^i and Q_{w}^i are the polarization factors of the rock matrix embedded by the water; and M is the total number of isolated pores.

3.1.2. Elastic moduli of dry rock

The dry rock skeleton comprises a rock matrix and empty pore space, which can be regarded as the mixture of connected dry pores and rock matrix. Assuming that the dry pore spaces also include stiff and soft pores, the bulk ($K_{\rm dry}$) and shear ($\mu_{\rm dry}$) moduli of dry rock can be calculated using the MT model (Mori and Tanaka, 1973):

$$K_{\text{dry}} = \frac{K_{\text{ma}}(1 - \varphi) + (1 - \eta)\varphi K_{\text{W}} \sum_{i=1}^{M} \nu_{i} P_{\text{W}}^{i}}{1 - \varphi + (1 - \eta)\varphi \sum_{i=1}^{M} \nu_{i} P_{\text{W}}^{i} + \eta\varphi \sum_{i=1}^{L} \nu_{i} \widehat{P}^{i}},$$
(5)

$$\mu_{\text{dry}} = \frac{\mu_{\text{ma}}(1 - \varphi)}{(1 - \varphi) + (1 - \eta)\varphi \sum_{i=1}^{M} \nu_{i} Q_{W}^{i} + \eta \varphi \sum_{i=1}^{L} \nu_{i} \widehat{Q}^{i}},$$
(6)

where v_i is the volume fraction for each inclusion i; \widehat{P}^i and \widehat{Q}^i represent polarization factors of ith dry connected pores, respectively; and L is the total types of dry connected pores.

3.1.3. Elastic moduli of saturated rock

Due to the heterogeneous distribution of gas and water in the pore spaces of tight sandstone reservoirs, the Wood equation fails to calculate the effective modulus of pore fluids. The Brie model (Brie et al., 1995) was utilized to calculate the bulk modulus of two-phase fluids:

$$K_{\rm fl} = (K_{\rm W} - K_{\rm g}) (1 - S_{\rm ge})^e + K_{\rm g},$$
 (7)

where $K_{\rm fl}$, $K_{\rm w}$, and $K_{\rm g}$ represent the bulk modulus of the pore—fluid mixture, water, and natural gas, respectively; e denotes the saturation index that reflects the characteristics of fluid distribution; and $S_{\rm ge}$ is the gas saturation in the partially connected pores determined by solving the equation proposed by Yan et al. (2016) with the assumption that the gas is injected into the water-saturated pore spaces and gradually replaces the water.

Once obtaining the elastic moduli of the rock matrix, dry rock framework, and pore fluids, the saturated rock moduli can be calculated using the Gassmann equation (Gassmann, 1951):

$$K_{\text{sat}} = K_{\text{dry}} + \frac{\left(1 - K_{\text{dry}} / K_0\right)^2}{\eta \varphi / K_{\text{fl}} + (1 - \eta \varphi) / K_0 - K_{\text{dry}} / K_0^2},$$
 (8)

$$\mu_{\mathsf{sat}} = \mu_{\mathsf{drv}},\tag{9}$$

where $K_{\rm sat}$ and $\mu_{\rm sat}$ are the bulk and shear moduli of saturated rock, respectively.

3.2. Numerical modeling

Understanding the effects of the microstructures on elastic behaviors is crucial for accurate lithology identification and fluid detection. Based on the partially connected double porosity model, we investigated the influences of the porosity, pore type, shale content, and pore connectivity on the elastic responses of tight sandstone reservoirs. The tight sandstone is assumed to be composed of clay and quartz, the pore fluid is a mixture of gas and water, and the aspect ratios of stiff and soft pores are set to 0.8 and 0.01 (Zhang et al., 2021), respectively. The elastic constants for each component used in the calculations are listed in Table 1.

3.2.1. Effect of pore type on elastic properties

Fig. 4 displays the elastic moduli and wave velocities varying with porosity and stiff pore fraction. As expected, both elastic

Table 1 Elastic properties of minerals and fluids for rock physics modeling.

Components	Bulk modulus, GPa	Shear modulus, GPa	Density, g/cm ³
Quartz ^a	38	44	2.65
Clay ^a	21	7	2.58
Water ^a	2.5	0	1.03
Gas ^b	0.03	0	0.125

Note: ^a Li and Zhang (2018); ^b Zillmer et al. (2005).

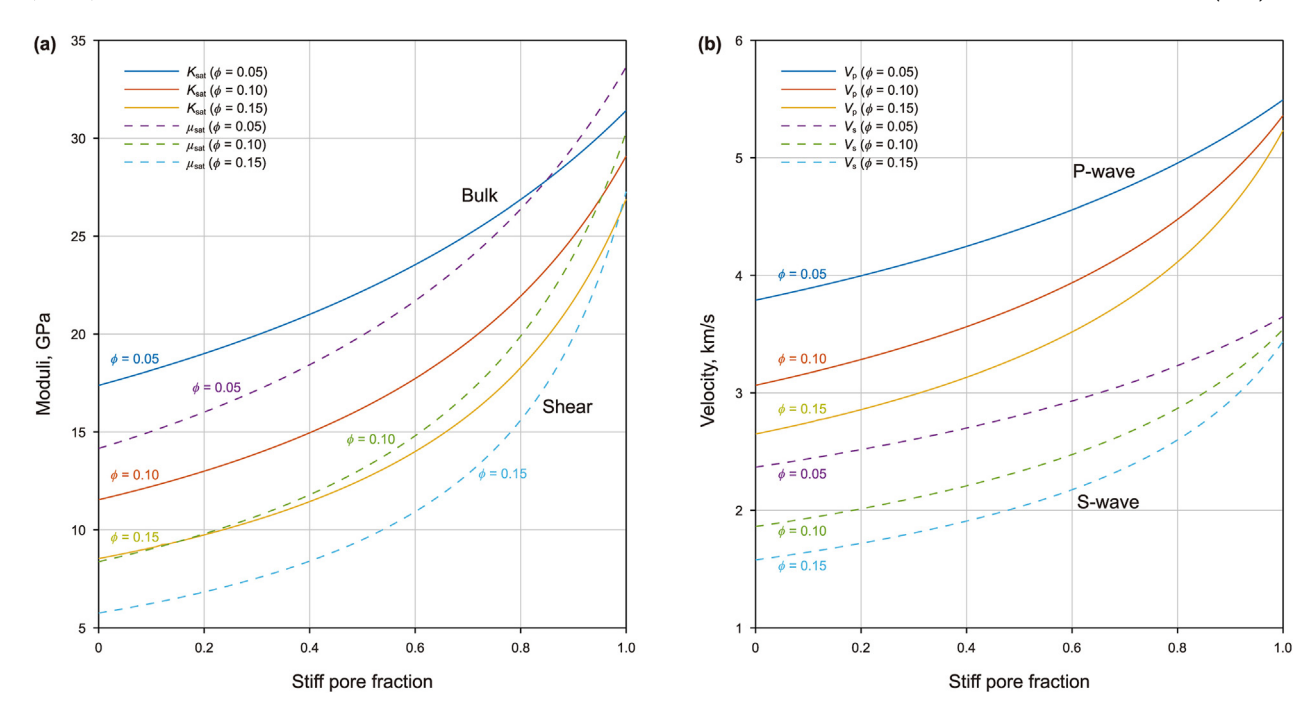


Fig. 4. Variations of elastic moduli (a) and velocities (b) of saturated rock with the volume fraction of the stiff pores for different porosities. Solid lines represent the bulk modulus (a) and P-wave velocity (b): dashed lines represent the shear modulus (a) and S-wave velocity (b).

properties of saturated rock decrease with the porosity but increase with the stiff pore fraction. In Fig. 4(a), although the stiff pore fraction exerts an apparent effect on the bulk and shear moduli, the increment of shear modulus is relatively larger than that of bulk modulus, especially at higher porosities and stiff pore fractions. As shown in Fig. 4(b), the variation trends of wave velocities are similar to those of elastic moduli, but the changes in P-wave velocity with stiff pore fraction are more significant than those in S-wave velocity for the three specific porosities. The abovementioned results suggest that the small number of soft pores (or cracks) can dramatically reduce wave velocities, and the impact of the pore type on the elastic responses of tight sandstone reservoirs gradually weakens with the decrease in porosity.

3.2.2. Effect of pore connectivity on elastic properties

An increasing number of digital core analyses and experimental studies show that the pore connectivity of tight sandstone is extremely complex due to the coexistence of connected pores. isolated pores, and partially connected pores (Mousavi, 2010; Ruiz and Cheng, 2010; Yan et al., 2016). Fig. 5 shows the saturated rock moduli and wave velocities as a function of pore connectivity and shale content. The porosity and stiff pore fraction are set to 10% and 50%, respectively. In Fig. 5(a), the bulk modulus shows a sharp decreasing trend with the pore connectivity coefficient, whereas the shear modulus decreases linearly with the increase in the pore connectivity coefficient. This comparison indicates that the pore connectivity mainly affects the fluid modulus and slightly affects the elastic moduli of the rock matrix and rock skeleton. For the given pore connectivity coefficient, the bulk and shear moduli of saturated rock decrease with the increase in shale content. As shown in Fig. 5(b), the P- and S-wave velocities decrease with the shale content increase and pore connectivity coefficient. Therefore, pore connectivity should be considered in rock physics modeling and reservoir characterization.

4. 3D RPT-based probabilistic estimation

The traditional 3D RPT inversion projects logging data or seismic-derived elastic parameters into the 3D template and searches the grid node nearest to the data point with the deterministic optimization algorithm. The estimated reservoir parameters are the gas saturation, porosity, and shale content corresponding to the optimal grid point. As we know, the estimation of reservoir parameters from seismic attributes is an inverse problem that is uncertain and non-unique. Thus, it is essential to quantify the uncertainty of inversion results. As such, a probabilistic estimation under the Bayesian framework is developed for quantifying reservoir properties and their corresponding uncertainties. Generally, the posterior probability distribution in Bayesian inference is the product of the prior distribution (the prior knowledge of model parameters) and likelihood function (the misfit between the observed and simulated data) given as (Tarantola, 2005)

$$q(\mathbf{m}|\mathbf{d}) = \frac{p(\mathbf{d}|\mathbf{m})p(\mathbf{m})}{\iiint p(\mathbf{d}|\mathbf{m})p(\mathbf{m})d\mathbf{m}},$$
(10)

where $\mathbf{m} = (S_{\rm g}, \varphi, V_{\rm sh})^{\rm T}$ and $\mathbf{d} = (\lg(I_{\rm P}), \lg(I_{\rm S}), \rho)^{\rm T}$ are the reservoir properties and measured data, respectively. If the model variables and observed data both follow Gaussian distribution, the prior information $p(\mathbf{m})$ and likelihood function $p(\mathbf{d}|\mathbf{m})$ can be written as

$$p(\mathbf{m}) \propto \exp\left\{-\frac{1}{2}(\mathbf{m} - \mathbf{m}_0)^{\mathrm{T}} \mathbf{C}_{\mathrm{M}}^{-1}(\mathbf{m} - \mathbf{m}_0)\right\},$$
 (11)

$$p(\mathbf{d}|\mathbf{m}) \propto \exp\left\{-\frac{1}{2}(f_{RPT}(\mathbf{m}) - \mathbf{d})^{\mathrm{T}}\mathbf{C}_{\mathrm{D}}^{-1}(f_{RPT}(\mathbf{m}) - \mathbf{d})\right\},\tag{12}$$

where \mathbf{m}_0 is the prior information; $f_{RPT}(\mathbf{m})$ represents the 3D RPT built by the partially connected double-porosity model; \mathbf{C}_M and \mathbf{C}_D are the model and data covariance matrix, respectively.

Combining Eqs. (10)–(12), the posterior probability distribution

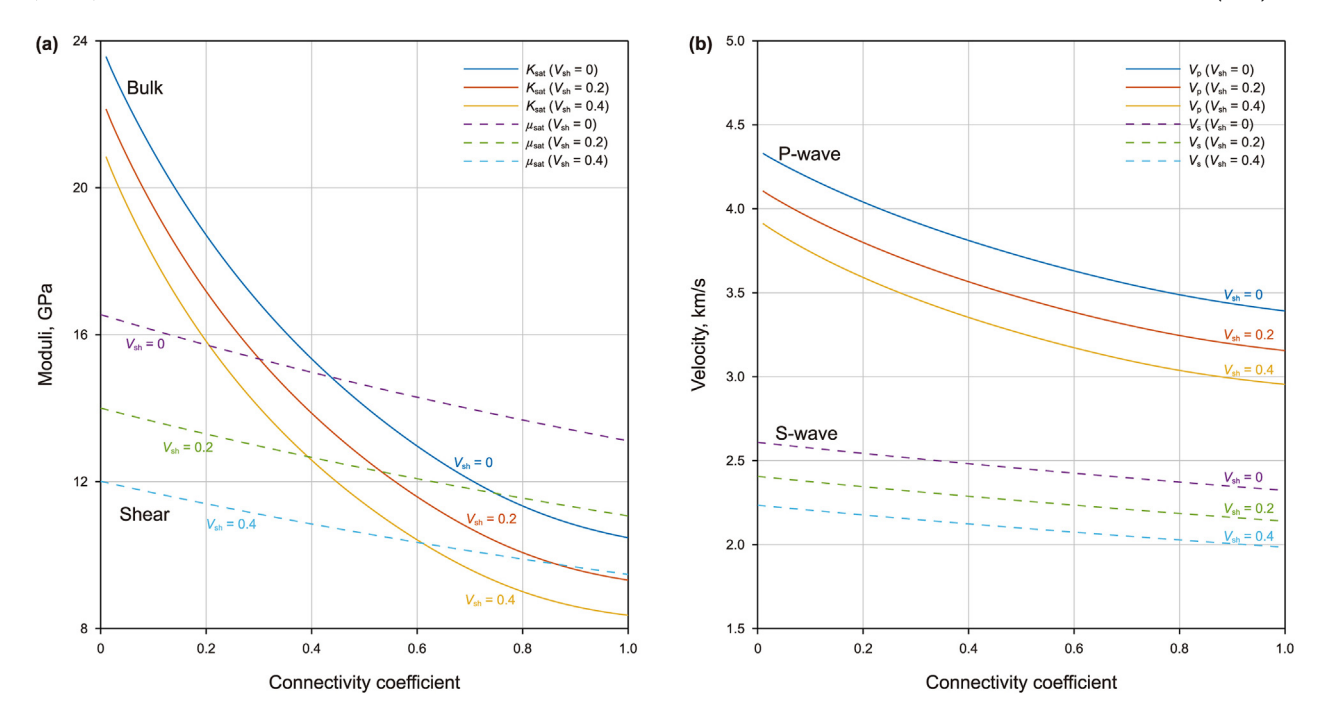


Fig. 5. Variations of elastic moduli (a) and velocities (b) of saturated rock with the pore connectivity coefficient for different shale contents. Solid lines represent the bulk modulus (a) and P-wave velocity (b); and dashed lines represent the shear modulus (a) and S-wave velocity (b).

of \mathbf{m} given the measured data \mathbf{d} can be written as

$$q(\mathbf{m}|\mathbf{d}) = N \exp[-J(\mathbf{m})] \tag{13}$$

where N is a normalization constant that satisfies the following equation: $\iiint N \exp[-J(\mathbf{m})] = 1$; $J(\mathbf{m})$ is the objective function given by

$$J(\mathbf{m}) = \frac{1}{2} \left[(f_{RPT}(\mathbf{m}) - \mathbf{d})^{T} \mathbf{C}_{D}^{-1} (f_{RPT}(\mathbf{m}) - \mathbf{d}) + (\mathbf{m} - \mathbf{m}_{0})^{T} \mathbf{C}_{M}^{-1} \right]$$

$$(\mathbf{m} - \mathbf{m}_{0})$$
(14)

In the case of an uninformative prior, the above objective function reduces to

$$J(\mathbf{m}) = \frac{1}{2} (f_{RPT}(\mathbf{m}) - \mathbf{d})^{\mathrm{T}} \mathbf{C}_{\mathrm{D}}^{-1} (f_{RPT}(\mathbf{m}) - \mathbf{d})$$
(15)

Then, the posterior probability in Eq. (13) is simplified into only a term describing the likelihood function multiplied by a normalized constant:

$$q(\mathbf{m}|\mathbf{d}) = N \exp\left\{-\frac{1}{2}\left[(f_{RPT}(\mathbf{m}) - \mathbf{d})^{\mathrm{T}}\mathbf{C}_{\mathrm{D}}^{-1}(f_{RPT}(\mathbf{m}) - \mathbf{d})\right]\right\},\tag{16}$$

The optimal model parameters can be found by maximizing the objective function in Eq. (14). To evaluate the uncertainty in the estimate of the specific model parameter m_i , a calculation of the marginal distribution is required (Tarantola, 2005):

$$q(m_i) = \int q(\mathbf{m}|\mathbf{d}) dm_1 dm_2 dm_3 \cdots dm_n$$
 (17)

Typically, it is infeasible to obtain an analytical solution in many practical applications. Hence, the numerical integration with respect to the other model parameters is often used to determine

the above marginal distribution. It should be noted that the numerical integration should be done on a grid dense enough to incorporate all the key features of the posterior distribution.

Assuming that the ranges of gas saturation, porosity, and shale content in the 3D RPT are $S_{\rm gmin} < S_{\rm g} < S_{\rm gmax}$, $\varphi_{\rm min} < \varphi < \varphi_{\rm max}$, and $V_{\rm shmin} < V_{\rm sh} < V_{\rm shmax}$, respectively, the normalized constant can be written as

$$\frac{1}{N} = \int_{S_{gmin}}^{S_{gmax}} \int_{\varphi_{min}}^{\varphi_{max}} \int_{V_{shmin}}^{V_{shmax}} exp[-J(S_g, \varphi, V_{sh})] dS_g d\varphi dV_{sh}, \tag{18}$$

The integral in Eq. (18) can be discretized and rewritten as follows:

$$\frac{1}{N} \approx \frac{\Delta S_{g} \Delta \varphi \Delta V_{sh}}{8} \sum_{k=1}^{K} \sum_{l=1}^{L} \sum_{m=1}^{M} \left\{ \exp \left[-J \left(S_{g,k}, \varphi_{l}, V_{sh,m} \right) \right] + \exp \left[-J \left(S_{g,k+1}, \varphi_{l+1}, V_{sh,m+1} \right) \right] \right\},$$
(19)

where $\Delta S_{\rm g} = \frac{S_{\rm gmax} - S_{\rm gmin}}{K-1}$, $\Delta \varphi = \frac{\varphi_{\rm max} - \varphi_{\rm min}}{L-1}$, and $\Delta V_{\rm sh} = \frac{V_{\rm shmax} - V_{\rm shmin}}{M-1}$ represent the intervals of reservoir parameters in 3D RPT. K, L, and M represent the number of grid points along the direction of gas saturation, porosity, and shale content, respectively.

Once the normalized constant is determined, the marginal probability density functions (PDFs) for each case can be found by Eq. (13). The corresponding marginal probability density distribution for gas saturation is given by

$$q(S_{g}) \approx N \frac{\Delta \varphi \Delta V_{sh}}{4} \sum_{l=1}^{L} \sum_{m=1}^{M} \left\{ \exp\left[-J(S_{g}, \varphi_{l}, V_{sh,m})\right] + \exp\left[-J(S_{g}, \varphi_{l+1}, V_{sh,m+1})\right] \right\},$$

$$(20)$$

and for porosity as

$$\begin{split} q(\varphi) &\approx N \frac{\Delta S_{\rm g} \Delta V_{\rm sh}}{4} \sum_{k=1}^K \sum_{m=1}^M \left\{ \exp \left[-J \left(S_{{\rm g},k}, \varphi, V_{{\rm sh},m} \right) \right] \right. \\ &\left. + \exp \left[-J \left(S_{{\rm g},k+1}, \varphi, V_{{\rm sh},m+1} \right) \right] \right\}, \end{split} \tag{21}$$

as well as for shale content as

$$q(V_{\rm sh}) \approx N \frac{\Delta S_{\rm g} \Delta \varphi}{4} \sum_{k=1}^{K} \sum_{l=1}^{L} \left\{ \exp\left[-J\left(S_{\rm g,k}, \varphi_{l}, V_{\rm sh}\right)\right] + \exp\left[-J\left(S_{\rm g,k+1}, \varphi_{l+1}, V_{\rm sh}\right)\right] \right\}.$$

$$(22)$$

It is thus possible to find a global maximum a posteriori solution for each reservoir parameter since we have obtained the exact marginal PDFs.

5. Application to actual data

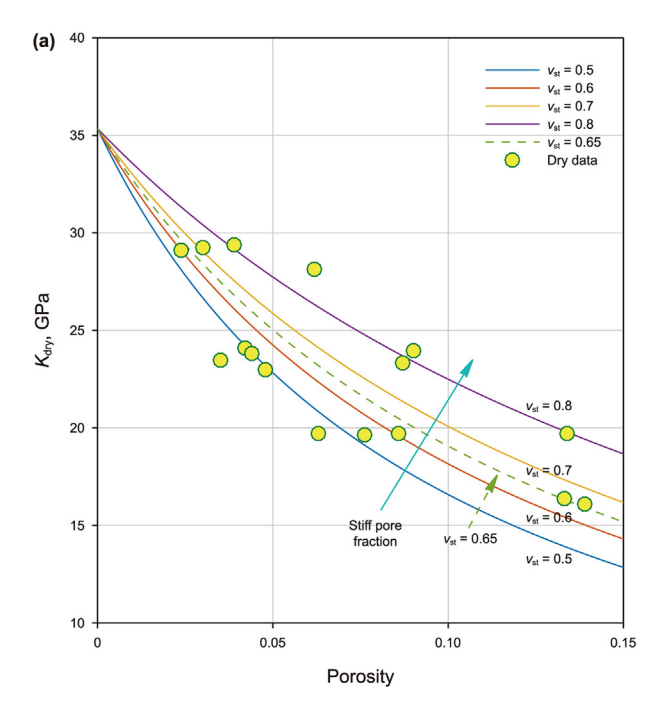
In the following section, we first validate the developed model with the ultrasonic laboratory data. Then, the 3D RPT-based probabilistic inversion scheme is tested by the well-log data. Finally, this approach is applied to predict reservoir properties from the prestack seismic-inverted elastic parameters.

5.1. Calibration of theoretical model

To determine the stiff pore fraction in the developed model, we compare the predicted elastic moduli of the dry rock with ultrasonic laboratory data of 16 sandstone samples in the target area reported by Yan et al. (2011). Concerning the uneven gas—water distribution in tight sandstones, the saturation index is set as 2.0. As shown in Fig. 6, the elastic moduli decrease with porosity but increase with the stiff pore fraction. It is found that most data points sit within a narrow range of stiff pore fraction from 50% to 80%, and the fluctuations of elastic moduli are mainly caused by the variations in mineral content and pore aspect ratio. Thus, the stiff pore fraction of 0.65 is recommended to use in this area. Although

the data are very scattered, the positive trend of stiff pore fraction with porosity indicated from model predictions and measurements is consistent. This is no surprise because the low-porosity layer often experiences strong compaction, decreasing the pore aspect ratio.

Fig. 7 compares the theoretical predictions with experimental results of varying gas saturations. The ultrasonic measurements are from Yan et al. (2016) and were acquired on a sandstone sample with varying water saturations. As we can see, the gas saturation and pore connectivity can also exercise appreciable impacts on elastic properties of tight sandstones apart from the aspect ratio and volumetric fraction of pores. As expected, the pore connectivity decreases both P- and S-wave velocities. This is predominantly attributed to the fact that, for a wave passing through porous rocks, the pore connectivity greatly promotes the pore fluid communication, and thus ensures the pore pressure equilibrated within a given relaxation time. However, the relationship between elastic wave velocities and gas saturation are much more complicated under different pore connectivity conditions. Typically, lower pore connectivity coefficients indicate the patchy saturation scenario, whereas higher pore connectivity coefficients favor the uniform saturation scenario. As a consequence, with the increase of pore connectivity coefficient, the P-wave velocity variation with gas saturation deviates from the upper patchy saturation boundary and is closed to the lower uniform saturation boundary. In contrast, the S-wave velocity decreases with gas saturation for lower pore connectivity coefficient, but it first increases and then decreases monotonically after exceeding a threshold value. This can be understood, because the pore connectivity not only impacts the bulk modulus of pore fluids, but also exerts an influence on the elastic moduli of rock matrix which might contribute to the change of Swave velocity. It can be observed from Fig. 7 that the measured data mostly follow the variation trend of model predictions with a pore connectivity coefficient of 0.55. This comparison conveys a message that the moderate pore connectivity coefficient indicating the mixing gas-water distribution may be applicable for tight sandstones when using the proposed model to interpret the sonic logs



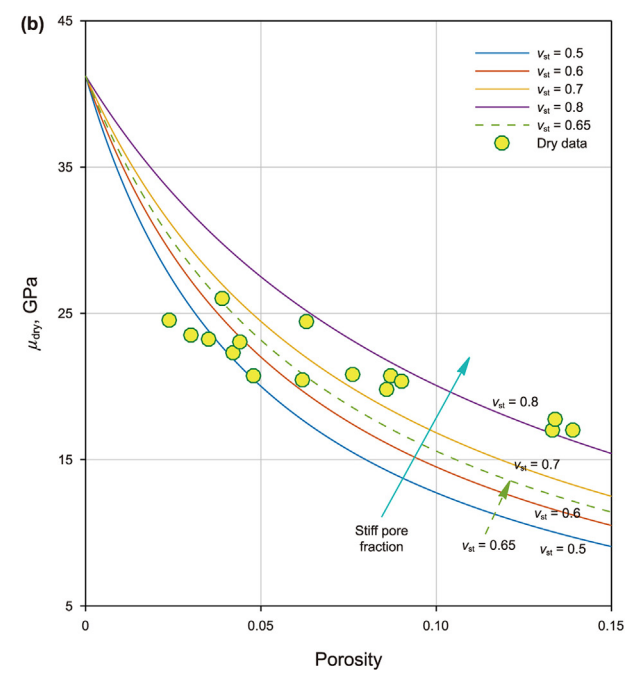


Fig. 6. The bulk (a) and shear moduli (b) of dry rock as a function of porosity for different fractions of stiff pores. The laboratory data used for comparison are from Yan et al. (2011).

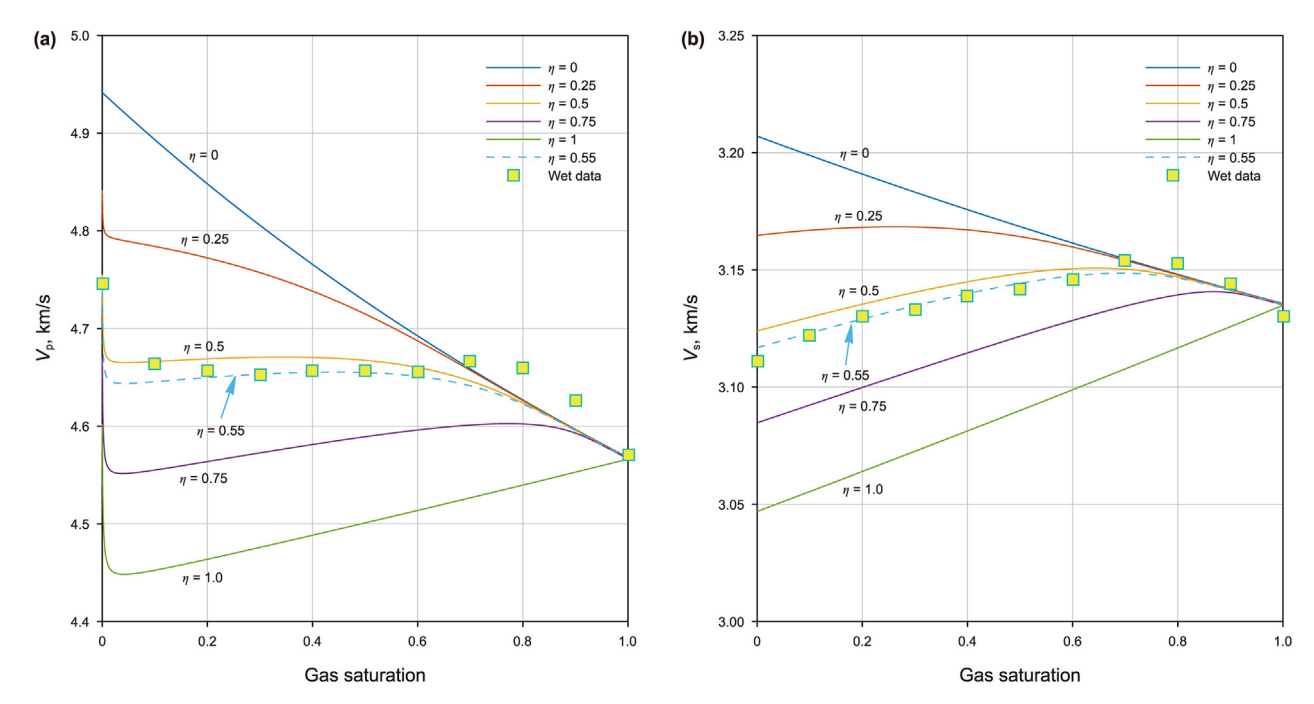


Fig. 7. The P- (a) and S-wave (b) velocities as a function of gas saturation for different pore connectivity coefficients. The laboratory data used for comparison are from Yan et al. (2016).

and seismic-inverted elastic properties.

5.2. Test of well-log data

Two wells in study area are utilized to verify the feasibility of the 3D RPT-based probabilistic inversion method. Among them, well Y1 is an industrial gas well whose production is 114,300 m³ per day, while the gas production of well Y2 is 8646 m³ per day. The reservoir type in the interval of interest is thin interbed of sandstone and mudstone. The cumulative sandstone thickness is 20–25 m for Y1 and approximately 25 m for Y2, respectively. The well-log analysis shows that the rock minerals consist of quartz and clay, and the pore fluid is a mixture of water and gas.

Based on the calibrated model, a 3D RPT that allows for the influences of gas saturation, porosity, and shale content on the P-wave impedance, S-wave impedance, and density is constructed. The elastic attributes all decrease with the increase in reservoir properties. Before the actual application of the 3D RPT, it is necessary to calibrate the template with well-log data. Fig. 8 compares the well Y2 logging data to the template. The red, blue, and green curves represent the constant gas saturation, porosity, and shale content lines, respectively. The distribution of the superimposed data points color-coded by the log interpretation is in good agreement with our templates, confirming the applicability of the 3D RPT in predicting gas saturation, porosity and shale content simultaneously.

Fig. 9 shows the probabilistic estimates of gas saturation, porosity and shale content from the elastic properties for well Y2. The black and blue curves represent the logging measurements or interpretation and the inversion results from the wave impedances and density based on 3D RPT. As shown in Fig. 9(a)-(c), the calculated elastic attributes are basically the same with the actual logging data. Fig. 9(d)-(f) compares the estimates of gas saturation, porosity and shale content with the logging interpretation results. It can be seen that the estimated porosity varies from 0 to 15% and the shale content varies from 0 to 35%, having a good agreement with the logging interpretations, except for the water-saturated

intervals at depths of 2170–2188 m and 2215–2228 m. By contrast, the estimated gas saturation ranging from 2% to 40% gives a good match with the interpretation at the gas-bearing intervals but overestimates at several water-saturated zones. To assess the uncertainties of the estimates, we introduce a 95% confidence region. Typically, the narrower the confidence intervals represent the more reliable estimates. By observing the width of the 95% confidence intervals, we can see that the estimation uncertainty of porosity is the smallest, the uncertainty of shale content is slightly larger, and the uncertainty of gas saturation is the largest. This is mainly because the elastic properties have low sensitivity to gas saturation compared with the porosity and shale content.

Fig. 10 compares the log interpretations and probabilistic estimations for well Y1. Fig. 10(a)-(c) illustrate that the calculated logarithmic P-wave and S-wave impedances and density match well with the observations. In Fig. 10(d)-(f), the estimated gas saturation varies from 0 to 100%, the porosity varies from 0 to 15%, and shale content ranges between 5% and 45%, achieving a satisfactory consistency with the logging interpretations, except for the water-saturated interval at depths of 2266-2310 m. The 95% confidence intervals are also calculated to evaluate the uncertainties of the inversion results. We can see that the confidence region of the porosity is the narrowest, the confidence region of gas saturation is relatively wide, and the confidence region of shale content is the widest, that is, the uncertainty of porosity > gas saturation > shale content. This phenomenon is primarily attributed to several factors, such as the measurement imperfection, the logging tool resolution difference, the unreasonable selection of rock mineral composition, pore structure heterogeneity, and the different sensitivities between reservoir properties and elastic parameters.

5.3. Application of seismic data

The proposed 3D RPT-based probabilistic inversion method is applied to a two-dimensional seismic profile through wells Y1 and Y2 in the studied area. The depth range of the target layer is 2100–2300 m, the corresponding travel time is 1046–1127 ms, and

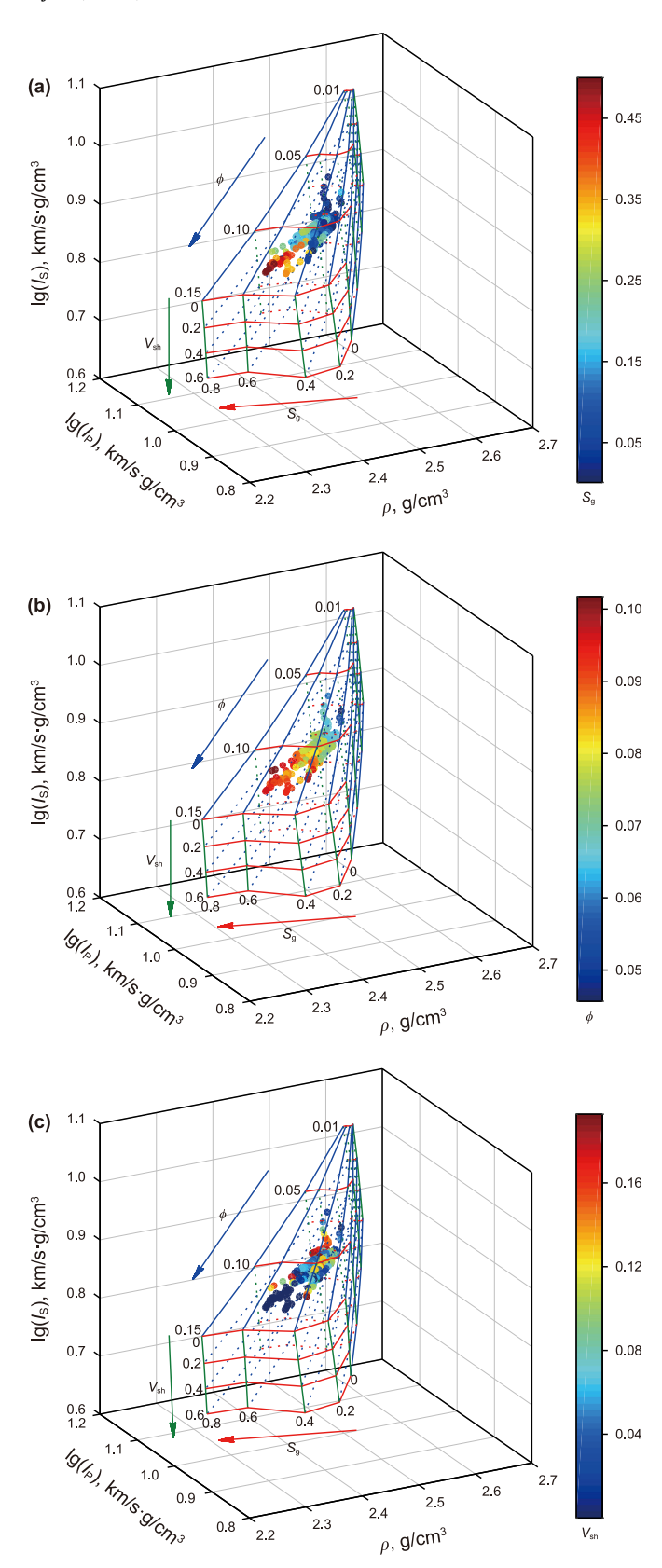


Fig. 8. Comparison between 3D RPT and log data. The data superimposed on the templates are from well Y2 in the Anyue gas field. The gas saturation ranges from 0 to 0.8, the porosity ranges from 0.01 to 0.15, and the shale content ranges from 0 to 0.6. The data are color-coded by **(a)** gas saturation, **(b)** porosity, and **(c)** shale content.

the CDP number is 2288 at well Y2; the depth range of the target layer is 2220–2370 m, the corresponding travel time is 1035–1102 ms, and the CDP number is 2807 at Y1 well. The P-wave impedance, S-wave impedance, and density are obtained from the pre-stack seismic data. Fig. 11 displays the results of the simultaneous AVO inversion. The estimated elastic parameters have a good correspondence with the logging curves, showing that the pre-stack seismic inversion can effectively characterize the spatial distribution of elastic properties and provide reliable data support for quantifying reservoir parameters.

Fig. 12 shows the probabilistic estimations of gas saturation, porosity, and shale content based on 3D RPT from the seismicextracted elastic parameters. It can be seen from Fig. 12(a) that the gas saturation estimates in the main reservoirs are relatively high at both the upper and lower parts of well Y1 but only at the lower part of well Y2, which is consistent with the logging interpretation. The lateral continuity of gas distribution at well Y1 is better than at well Y2. The estimated profile of gas saturation is comparable to the actual drilling information. Fig. 12(b) shows the inverted porosity profile through wells Y1 and Y2. Compared with well Y2, well Y1 shows higher porosities, indicating better connectivity and higher gas storage potential for well Y1. Moreover, the vertical heterogeneity of well Y2 is stronger than well Y1. Fig. 12(c) shows the inverted profile of shale content. It can be seen that the shale content of the gas-bearing layers at well Y1 is lower than that at well Y2, which also shows a good fit with the logging interpretation. Overall, the seismic inversion results of reservoir properties are consistent with well-log data and actual gas production results, verifying our method's effectiveness.

6. Discussion

The key to accurate characterization of tight sandstone reservoirs largely depends on establishing a reliable relationship between reservoir parameters and elastic responses. In this study, we propose a partially connected double porosity model for tight gas sandstone reservoirs. This model first assumes that all pores are divided into connected and isolated pores. Typically, the waveinduced pore pressure among connected pores is easier to reach equilibrium through fluid communication, whereas fluid in the isolated pores does not exchange with the outside (Yan et al., 2016). The fluid-saturated isolated pores are considered part of the rock matrix, while the connected pores are the inclusions embedded into the background matrix. Unlike the connected pores filled with the gas-water mixture, the isolated pores are supposed to be only saturated with water. A plausible explanation for this assumption is that gas moves upward via the buoyancy and capillary force and preferentially accumulates in the permeable pores by replacing the water.

In addition to pore connectivity, the pore structures are also simplified into soft and stiff pores, both of which have fixed aspect ratios. In addition, the concentration of stiff pores is required to be identical in both connected and disconnected cases. However, in real rocks, the pores distribute randomly and exhibit irregular microstructures with a possible distribution of pore aspect ratios. Some advanced characterization technologies, such as digital image analysis (e.g., scanning electron microscope and micro-CT scanning) (Su et al., 2022) and digital rock physics (Yang et al., 2023a; Zhao et al., 2021a), can be used to assist in characterizing the pore structures of tight sandstones. Another issue is the consideration of rock mineral components. Due to lack of the elemental capture spectroscopy and LithoScanner logs, we only consider a simple mineralogical mixture of quartz-clay and calculate the shale content from Gama Ray log. To improve the accuracy of prediction results, the mineral constituent selection should be referenced to

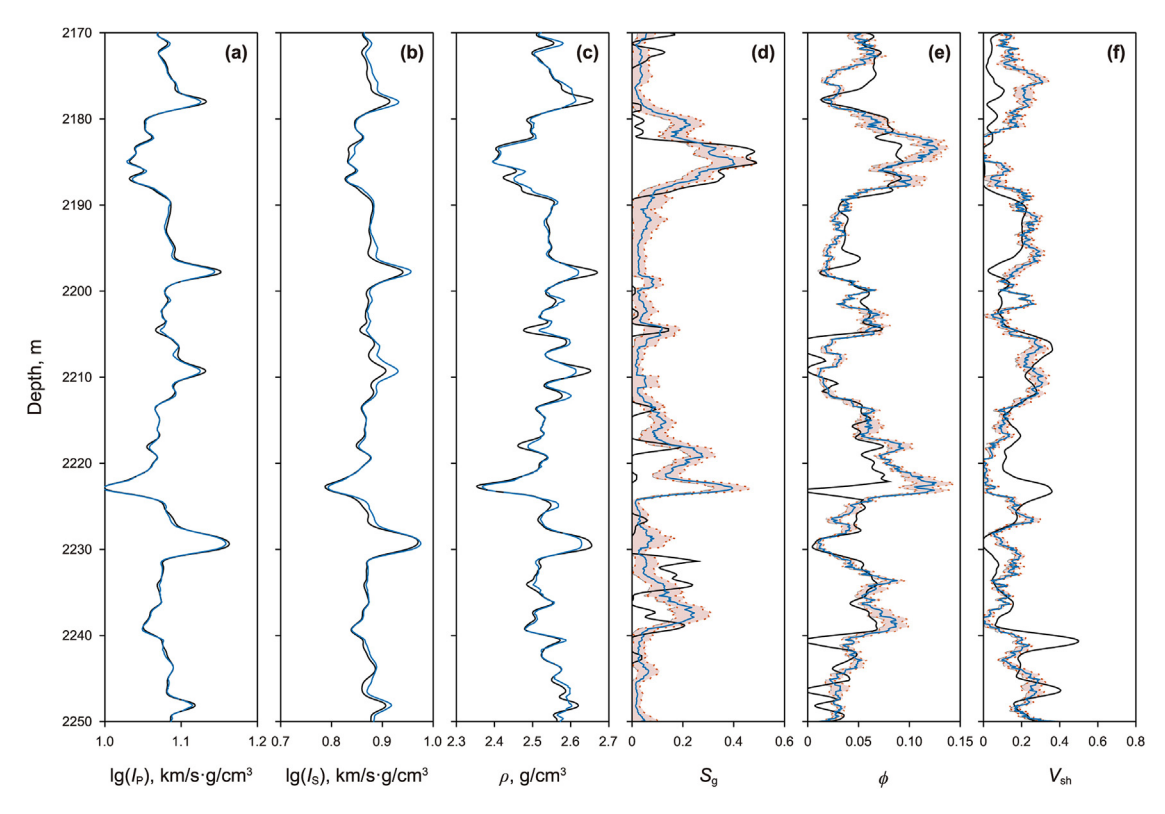


Fig. 9. Comparisons of the 3D RPT-based probabilistic estimations with actual data for well Y2. (a) Logarithmic P-wave impedance; (b) logarithmic S-wave impedance; (c) density; (d) gas saturation; (e) porosity; (f) shale content. The black lines represent the logging measurements or interpretations, the blue lines represent the estimations, and the shaded parts represent the 95% confidence intervals of the inversion results.

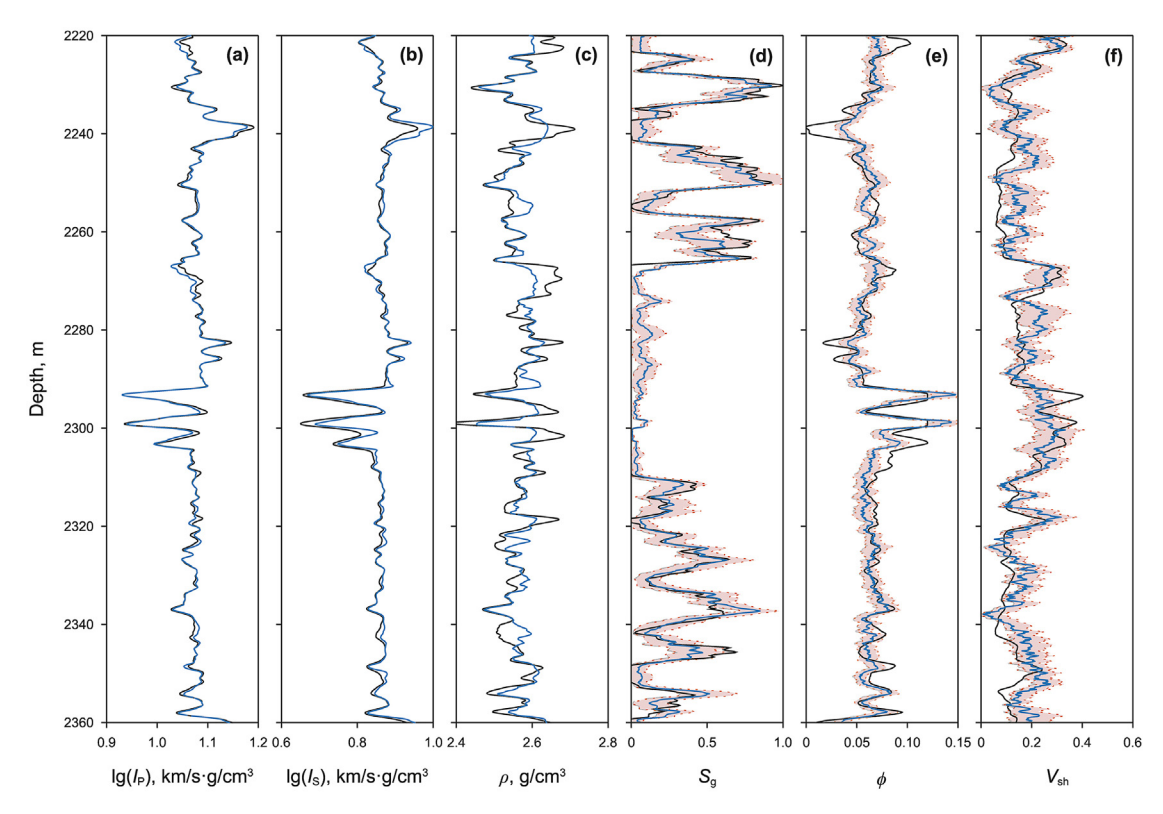
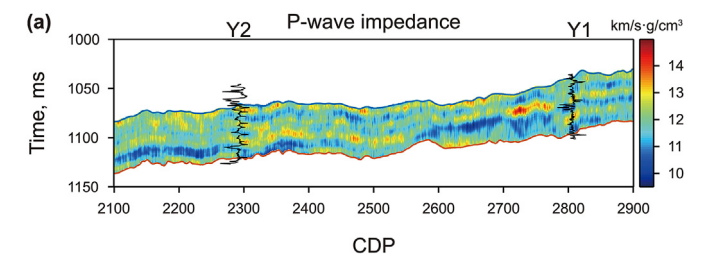
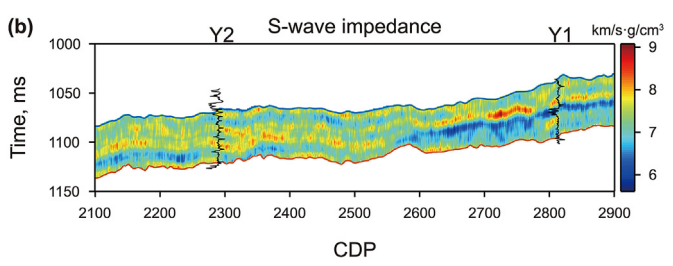


Fig. 10. Comparisons of the 3D RPT-based probabilistic estimations with actual data for well Y1. (a) Logarithmic P-wave impedance; (b) logarithmic S-wave impedance; (c) density; (d) gas saturation; (e) porosity; (f) shale content. The black lines represent the logging measurements or interpretations, the blue lines represent the estimations, and the shaded parts represent the 95% confidence intervals of the inversion results.





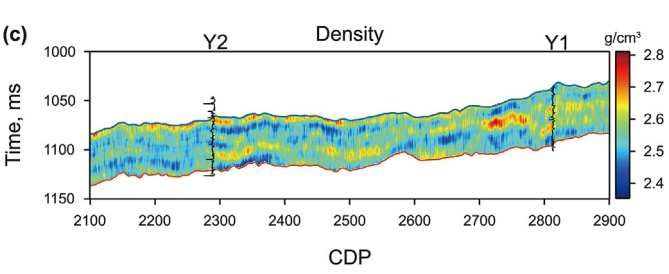
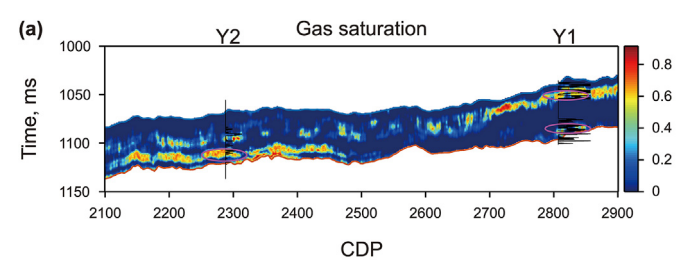
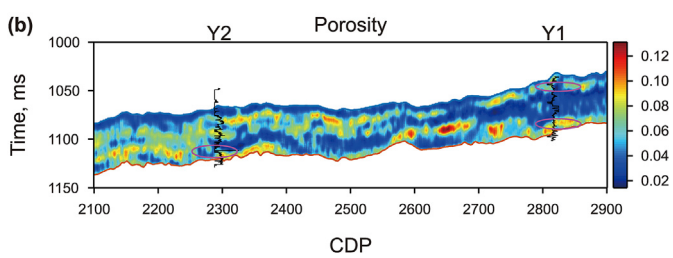


Fig. 11. Pre-stack seismic inversion profiles of P-wave impedance **(a)**, S-wave impedance **(b)**, and density **(c)** with the corresponding log curves.





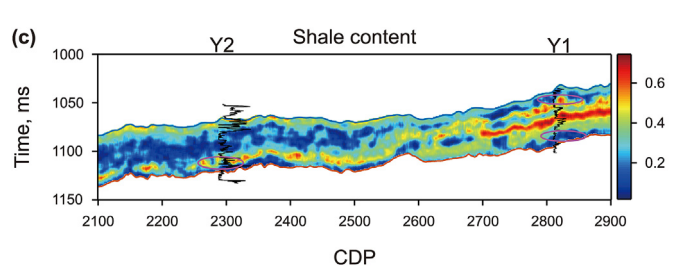


Fig. 12. The 3D RPT-based probabilistic estimations of gas saturation (a), porosity (b), and shale content (c) with the corresponding logging interpretation curves.

the XRD analysis and petrophysical interpretation in real application. Also, the anisotropy induced by the aligned fractures and preferential arrangement of clay minerals is ignored in our modeling, which limits our model to describe the deep-buried tight sandstone reservoirs with high heterogeneity. Therefore, it is necessary to develop an anisotropic partially connected variable-matrix multi-pore model to improve the accuracy of tight sandstone reservoir prediction.

3D RPT is an effective means to transform elastic attributes into physical parameters. It should be pointed out that the constructed 3D RPT does not consider the different correlations between elastic responses and reservoir parameters at the core, log, and seismic scales. Therefore, the multi-scale 3D RPT should be established based on the frequency-dependent rock-physics model instead of the Gassmann equation (Yang and Zhang, 2002; Tang, 2011; Ba et al., 2017). In addition, the tight sandstone reservoirs often have strong pore structure or fluid distribution heterogeneities, making it necessary to build an anisotropic 3D RPT to enhance the applicability and reliability of the template. Provided that the rock mineral component and its volumetric fraction do not vary widely in the target intervals, the 3D RPT can be adapted to predict the reservoir properties and the volume fraction of stiff pores or the pore connectivity. The reservoir property estimation is an ill-posed inverse problem with non-unique solutions. To evaluate the uncertainties in the estimates, the probabilistic estimation, instead of deterministic optimization, is used to search for the optimal solution from the maximum marginal probability that reflects the best fitting between the projected data point and the nearest node on the 3D RPT. Overall, the 3D RPT-based probabilistic inversion method not only predicts reservoir properties from elastic properties but also quantifies their corresponding uncertainties, showing good promise in reservoir characterization.

Quantitative characterization of tight sandstone reservoirs can not only use the model-driven inversion method introduced in this paper, but also can use the data-driven method to estimate reservoir properties. With the technological advances of artificial intelligence and machine learning, an increasing number of data-driven approaches have been introduced into the field of applied geophysics, such as shear wave estimation (Wang et al., 2022), reservoir property prediction (Zhang et al., 2022a; Yang et al., 2023b), fluid and lithofacies classification (Zhao et al., 2021b), seismic impedance inversion (Su et al., 2023; Zhang et al., 2022b) and seismic data denoising (Yu et al., 2019). However, one of the major challenges in geophysical applications of the data-driven methods is how to ensure the generalization ability and predictive performance of the machine learning or deep learning algorithm when facing the lack of labeled training data (Chen et al., 2021).

7. Conclusion

Considering the complex pore structure and pore connectivity, we propose a partially connected double pore model based on the SCA, MT, and Gassmann equation. Our new model investigates the dependence of elastic responses on pore type and connectivity. Modeling results show that the elastic moduli and velocities both increase with the fraction of stiff pores but decrease with pore connectivity. More importantly, such influences largely rely on porosity and mineral composition. Furthermore, the investigation also indicates that the pore type significantly impacts shear modulus, whereas pore connectivity more appreciably impacts the bulk modulus of saturated rock. The calibration of the developed model with experimental data enables us to determine the pore connectivity coefficient and the volume fraction of stiff pores, and to improve the accuracy of model predictions. Based on the

calibrated model, we establish a 3D RPT to analyze the linkage between reservoir and elastic properties. Under the Bayesian theory framework, a 3D RPT-based probabilistic inversion method is proposed to predict reservoir parameters and their uncertainties. The application to well-log data shows that the estimated gas saturation and porosity satisfactorily match the logging interpretations, whereas the shale content is slightly overestimated at some reservoir intervals. The seismic inversion results are consistent with logging interpretations and gas production results, confirming the feasibility of our approach in reservoir quality prediction for tight gas sandstones.

Acknowledgments

This work was supported by the National Natural Science Foundation of China (42104121) and the Scientific Research and Technology Development Project of the CNPC (2021DJ0606).

References

- Ba, J., Xu, W.H., Fu, L.Y., et al., 2017. Rock anelasticity due to patchy saturation and fabric heterogeneity: a double double-porosity model of wave propagation. J. Geophys. Res. Solid Earth 122 (3), 1949–1976. https://doi.org/10.1002/2016/B013882.
- Berryman, J.G., 1980. Long-wavelength propagation in composite elastic media II. Ellipsoidal inclusions. J. Acoust. Soc. Am. 68 (6), 1820–1831. https://doi.org/10.1121/1.385172.
- Brie, A.F., Pampuri, A.F., Marsala, F., et al., 1995. Shear sonic interpretation in gasbearing sands. In: SPE Annual Technical Conference and Exhibition,. https:// doi.org/10.2118/30595-MS, 701-710.
- Chen, Y.Y., Zhao, L.X., Pan, J.G., et al., 2021. Deep carbonate reservoir characterisation using multi-seismic attributes via machine learning with physical constraints. J. Geophys. Eng. 18 (5), 761–775. https://doi.org/10.1093/jge/gxab049.
- Gassmann, F., 1951. Elastic waves through a packing of spheres. Geophysics 16 (4), 673–685. https://doi.org/10.1190/1.1437718.
- Hill, R., 1952. The elastic behaviour of a crystalline aggregate. Proc. Phys. Soc. 65 (5), 349. https://doi.org/10.1088/0370-1298/65/5/307.
- Lai, J., Wang, G.W., Cai, C., et al., 2018. Diagenesis and reservoir quality in tight gas sandstones: the fourth member of the upper triassic Xujiahe Formation, central Sichuan Basin, Southwest China. Geol. J. 53 (2), 629–646. https://doi.org/ 10.1002/gi.2917.
- Lai, J., Wang, G.W., Fan, Z., et al., 2016. Insight into the pore structure of tight sandstones using NMR and HPMI measurements. Energy & Fuels 30 (12), 10200–10214. https://doi.org/10.1021/acs.energyfuels.6b01982.
- Li, H.B., Zhang, J.J., 2018. Well log and seismic data analysis for complex porestructure carbonate reservoir using 3D rock physics templates. J. Appl. Geophys. 151, 175–183. https://doi.org/10.1016/j.jappgeo.2018.02.017.
- Li, X.Z., Guo, Z.H., Wan, Y.J., et al., 2017. Geological characteristics and development strategies for Cambrian Longwangmiao Formation gas reservoir in Anyue gas field, Sichuan Basin, SW China. Petrol. Explor. Dev. 44 (3), 428–436. https://doi.org/10.1016/S1876-3804(17)30049-6.
- Liu, Q., Yin, X.Y., Li, C., 2015. Prediction method of rock elastic modulus of tight sandstone reservoir with unconnected pores. Geophys. Prospect. Pet. 54 (6), 635–642. https://doi.org/10.3969/J.ISSN.1000-1441.2015.06.001 (in Chinese).
- Luo, Y.N., Huang, H.D., Jakobsen, M., et al., 2019. Prediction of porosity and gas saturation for deep-buried sandstone reservoirs from seismic data using an improved rock-physics model. Acta Geophys. 67, 557–575. https://doi.org/ 10.1007/s11600-019-00274-6.
- Mori, T., Tanaka, K., 1973. Average stress in matrix and average elastic energy of materials with misfitting inclusions. Acta Metall. 21 (5), 571–574. https:// doi.org/10.1016/0001-6160(73)90064-3.
- Mousavi, M.A., 2010. Pore-scale Characterization and Modeling of Two-phase Flow in Tight Gas Sandstones. University of Texas at Austin, Texas, Ph.D Dissertation.
- Pan, H.J., Li, H.B., Cai, S.J., et al., 2020. An improved Pride model for S-Wave velocity prediction in tight gas sandstones. In: 82nd EAGE Annual Conference & Exhibition. https://doi.org/10.3997/2214-4609.202010933.
- Pan, H.J., Li, H.B., Grana, D., et al., 2019. Quantitative characterization of gas hydrate bearing sediment using elastic-electrical rock physics models. Mar. Petrol. Geol. 105, 273–283. https://doi.org/10.1016/j.marpetgeo.2019.04.034.

Pang, M.Q., Ba, J., Carcione, J.M., 2021. Characterization of gas saturation in tight-sandstone reservoirs with rock-physics templates based on seismic Q. J. Energy Eng. 147 (3). https://doi.org/10.1061/(ASCE)EY.1943-7897.0000761.

- Ruiz, F., Cheng, A., 2010. A rock physics model for tight gas sand. Lead. Edge 29 (12), 1484–1489. https://doi.org/10.1190/1.3525364.
- Shen, F., Yue, L., Liu, Z.L., et al., 2021. Heterogeneity of tight sandstone reservoirs based on fractal theory: the Xu-6 member of Xujiahe Formation in Guang'an area, central Sichuan Basin. Arabian J. Geosci. 14, 1–14. https://doi.org/10.1007/ s12517-021-07851-4
- Smith, T.M., Sayers, C.M., Sondergeld, C.H., 2009. Rock properties in low-porosity/low-permeability sandstones. Lead. Edge 28 (1), 48–59. https://doi.org/10.1190/1.3064146.
- Su, Y., Zha, M., Jiang, L., et al., 2022. Pore structure and fluid distribution of tight sandstone by the combined use of SEM, MICP and X-ray micro-CT. J. Petrol. Sci. Eng. 208, 109241. https://doi.org/10.1016/j.petrol.2021.109241.
- Su, Y.Q., Cao, D.P., Liu, S.Y., et al., 2023. Seismic impedance inversion based on deep learning with geophysical constraints. Geoenergy Science and Engineering 225, 211671. https://doi.org/10.1016/j.geoen.2023.211671.
- Tan, W.H., Ba, J., Fu, L.Y., et al., 2021. 3D rock physics template analysis and "sweet spot" prediction of Longmaxi-Wufeng organic-rich shale. Chin. J. Geophys. 64 (8), 2900–2915. https://doi.org/10.6038/cjg202100380 (in Chinese).
- Tang, X., 2011. A unified theory for elastic wave propagation through porous media containing cracks-An extension of Biot's poroelastic wave theory. Sci. China Earth Sci. 54 (9), 1441–1452. https://doi.org/10.1007/s11430-011-4245-7.
- Tarantola, A., 2005. Inverse Problem Theory and Methods for Model Parameter Estimation. Society for Industrial Mathematics.
- Vernik, L., Landis, C., 1996. Elastic anisotropy of source rocks: implications for hydrocarbon generation and primary Migration1. AAPG (Am. Assoc. Pet. Geol.) Bull. 80 (4), 531–544. https://doi.org/10.1306/64ED8836-1724-11D7-8645000102C1865D.
- Wang, J., Cao, J.X., Zhao, S., et al., 2022. S-wave velocity inversion and prediction using a deep hybrid neural network. Sci. China Earth Sci. 65 (4), 1–18. https://doi.org/10.1007/s11430-021-9870-8.
- Yan, X.F., Li, X.M., Wei, X., et al., 2016. Rock physics modeling in partially connected porous medium. In: 86th SEG Technical Program Expanded Abstracts. https:// doi.org/10.1190/segam2016-13951657.1.
- Yan, X.F., Yao, F.C., Cao, H., et al., 2011. Analyzing the mid-low porosity sandstone dry frame in central Sichuan based on effective medium theory. Appl. Geophys. 8 (3), 163–170. https://doi.org/10.1007/s11770-011-0293-1.
- Yang, D.H., Zhang, Z.J., 2002. Poroelastic wave equation including the Biot/Squirt mechanism and the solid/fluid coupling anisotropy. Wave Motion 35, 223–245. https://doi.org/10.1016/S0165-2125(01)00106-8.
- Yang, N.X., Li, G.F., Zhao, P.Q., et al., 2023a. Porosity prediction from pre-stack seismic data via a data-driven approach. J. Appl. Geophys. 211, 104947. https://doi.org/10.1016/j.jappgeo.2023.104947.
- Yang, Y.F., Horne, R.N., Cai, J.C., et al., 2023b. Recent advances on fluid flow in porous media using digital core analysis technology. Advances in Geo-Energy Research 9 (2), 71–75. https://doi.org/10.46690/ager.2023.08.01.
- Yu, S., Ma, J., Wang, W., 2019. Deep learning for denoising. Geophysics 84 (6), V333–V350. https://doi.org/10.1190/geo2018-0668.1.
- Zhang, H.H., Zhang, G.Z., Gao, J.H., et al., 2022a. Seismic impedance inversion based on geophysical-guided cycle-consistent generative adversarial networks. J. Petrol. Sci. Eng. 218, 111003. https://doi.org/10.1016/j.petrol.2022.111003.
- Zhang, J.J., Liu, Z.F., Zhang, G.Z., et al., 2022b. Simultaneous prediction of multiple physical parameters using gated recurrent neural network: porosity, water saturation, shale content. Front. Earth Sci. 10, 984589. https://doi.org/10.3389/ feart.2022.984589.
- Zhang, J.J., Zeng, Q.C., Yin, X.Y., et al., 2021. Multiple-porosity variable critical porosity model and pore structure characterization. Chin. J. Geophys. 64 (2), 724–734. https://doi.org/10.6038/cjg2021M0675 (in Chinese).
- Zhao, J.G., Pan, J.G., Hu, Y.M., et al., 2021a. Digital rock physics-based studies on effect of pore types on elastic properties of carbonate reservoir Part 1: imaging processing and elastic modelling. Chin. J. Geophys. 64 (2), 656–669. https://doi.org/10.6038/cjg202100228 (in Chinese).
- Zhao, L.X., Zou, C.F., Chen, Y.Y., et al., 2021b. Fluid and lithofacies prediction based on integration of well-log data and seismic inversion: a machine-learning approach. Geophysics 86 (4), M151–M165. https://doi.org/10.1190/geo2020-05211
- Zillmer, M., Reston, T., Leythaeuser, T., et al., 2005. Imaging and quantification of gas hydrate and free gas at the Storegga slide offshore Norway. Geophys. Res. Lett. 32 (4), 1–4. https://doi.org/10.1029/2004GL021535.
- Zou, C.N., Gong, Y.J., Tao, S.Z., et al., 2013. Geological characteristics and accumulation mechanisms of the "continuous" tight gas reservoirs of the Xu2 Member in the middle-south transition region, Sichuan Basin, China. Petrol. Sci. 10, 171–182. https://doi.org/10.1007/s12182-013-0264-7.